INFLUENCE OF TURBULENCE SCALE AND SHAPE OF LEADING EDGE ON FST-INDUCED LAMINAR-TURBULENT TRANSITION

M.V. Ustinov*, A.A. Uspensky*
*** Central Aerohydrodynamic Institute (TsAGI)**
ustinov@tsagi.ru; skvortsov@aerocentr.msk.su
Keywords: *laminar-turbulent transition*, *boundary layer*

Abstract

Influence of turbulence scale and shape of leading edge on laminar turbulent transition in the boundary layer on the flat plate subjected to free-stream turbulence (FST) was studied experimentally. It was found that length scale of turbulence has a dramatic effect on disturbances growth in the boundary layer at the sharp-nosed plate. Enhanced receptivity of blunt-nosed plate boundary layer to FST was demonstrated. New linear receptivity theory describing these findings of experiment was developed.

1 Introduction

The effect of free-stream turbulence (FST) on laminar turbulent transition in a boundary layer has become of great interest during the last decade. General consensus is that boundary layer disturbances in this conditions grow proportionally to Reynolds number based on the boundary layer thickness. It means that transition Reynolds number should be determined by the turbulence intensity only. However the discrepancy in published observations of transition is substantial (see [1]). From this it follows that transition location is not entirely determined by turbulence level, but it is influenced by several factors which are not entirely understood. The most obvious is the influence of length scale of FST. Despite of several studies focused on this factor there is no general agreement among scientists about influence of turbulence scale on transition. Theoretical work of M. Goldstein *et al.* [2] showed that another important factor should be the shape of leading edge. Additional amplification of normal to edge vorticity by means of vortex lines stretching predicted by [2] should move transition on blunted body upstream. However, there are no experimental validations of this effect. Present work is devoted to investigation of influence of FST scale and shape of leading edge on the transition in flat-plate boundary layer.

2 Experiment

At first influence of turbulence scale and shape of leading edge on FST induced laminar-turbulent transition in the flat plate boundary layer was studied experimentally. The experiment was performed in the low-turbulence direct-flow wind tunnel T-36 I of TsAGI. The test section is 2.6 m long, 0.5 m wide and 0.35 m high, and is preceded by a 12:1 contraction. General outline of experimental setup is shown in Fig. 1. Development of disturbances initiated by free-stream turbulence in the boundary layer on the flat plate was investigated. The plate of 1810 mm long, 500 mm wide and 20 mm thick was made from plexiglas and had two edges of different shape. In order to investigate the influence of shape of leading edge on laminar-turbulent transition it was installed onward one of the edges. The first sharp edge had 8:1 semi-elliptical profile. Contour of the second blunt edge was designed specially to obtain non-separated flow for maximal radius of leading edge. The radius of sharp edge was r_1=1.25mm, the blunt edge has radius r_2=5.31mm. The flow around the edges was adjusted to be symmetric using flap mounted above the plate near its trailing edge. To control the stagnation point position the leading edges were drained and static pressure distribution over the surface was measured. Mean streamwise velocity in boundary layer and its pulsations were measured by DISA 55M01 hot-wire anemometer. Experiment was performed for two values of flow velocity 8 and 16 m/sec.

(a)

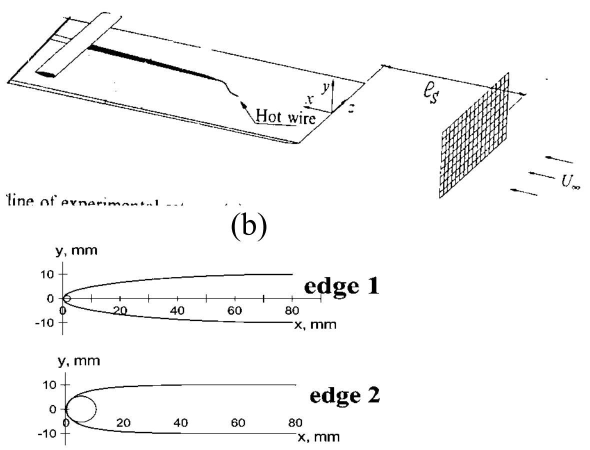

Fig. 1. General outline of experiment (a); shapes of leading edges (b)

Enhanced turbulence level in the test section was generated by three grids of different mesh size and diameter of wire installed upstream the plate. The distance from each mesh to the leading edge was adjusted to obtain turbulence level *Tu*=1.3% at the leading edge position. Integral scales of turbulence generated by the grids were roughly equal to 3, 6, and 9 mm for grids #1,2,3 and do not depend from flow velocity. Turbulence level was almost the same for all grids and changes in range $1.31 \pm 0.1\%$.

R.m.s. velocity pulsations as functions of Reynolds number $R = \sqrt{\nu x / u_\infty}$ obtained for different combinations of leading edge shape, flow velocity and scale of turbulence are shown in Fig. 2. It demonstrates, that in accordance with prediction of theory transition on the blunt-nosed plate occurs earlier compared with transition on sharp-nosed one. Development of pulsations on the sharp-nosed plate depends substantially from both turbulent scale and flow velocity. Enhance of free-stream velocity results in increase of boundary layer perturbations. Dependence of pulsations growth from turbulence scale is non-monotonic, with maximal growth occurs for intermediate scale 6 mm comparable with boundary layer thickness. Pulsations from small-scale turbulence in flow with u_∞=8 m/sec do not grow permanently, but reache maximum and decay downstream.

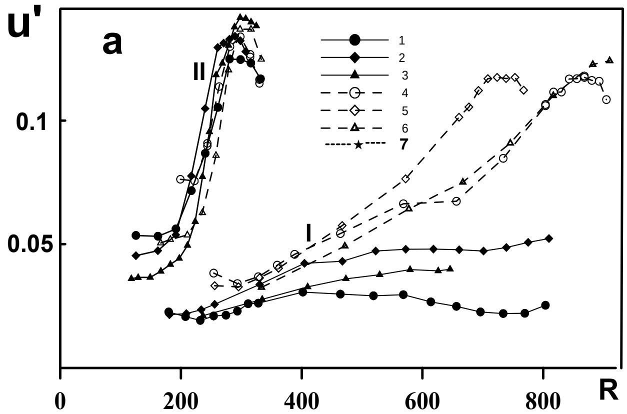

Fig. 2. Pulsations in the boundary layer on the plate with sharp (I) and blunt (II) leading edge for *Tu*=1.3% and different turbulence scale in free stream; (1) – L=3 mm (grid 1), (2) – L=6mm (grid 2), (3) – L=9 mm (grid 3). Results for U=8m/sec and 16m/sec are shown by solid and dashed lines.

Linear theory of boundary layer receptivity developed by Leib, Wundrow & Goldstein [3] states that development of r.m.s. pulsations in boundary layer is described by the universal law

$$\frac{\sqrt{<u'^2>}}{TuR_L} = F\left(\frac{R}{R_L}\right) \qquad (1)$$

where R_L - is Reynolds number based on integral scale of turbulence *L*.

Results of present experiment scaled in this way together with data of Westin *et al*. [1] and theoretical universal amplification curve computed in [3] are presented in Fig.3. It shows that theory [3] strongly underestimates magnitude of pulsations and gives the credible result only for the case of grid#1 and u_∞*=8m/sec*. In spite of the fact that scaling proposed by Leib, Wundrow & Goldstein [3] have failed, the regular trend, such as increase of normalized pulsations amplitude with growth of turbulence Reynolds number $R_t = Tuu_\infty L / \nu$

is clearly seen. To highlight this trend the experimental data are subdivided into four groups. The first group includes results for grid#1, u_∞=*8m/sec* and R_t =21, second group includes four experimental cases in which R_t are close to 50, the third group includes results of Westin *et al.* for flow velocity *8 m/sec* and case of grid #2, u_∞=*16m/sec* for which R_t=85-95, the last group consists from the single case of grid #3 and u_∞=*16m/sec* for which R_t=125. These groups of data are marked by blue, violet, orange and red colours. Fig.3 shows that the data from each group are close to each other instead of difference of flow velocity and turbulence scale and growth rate of pulsations grows monotonically with increase of R_t.

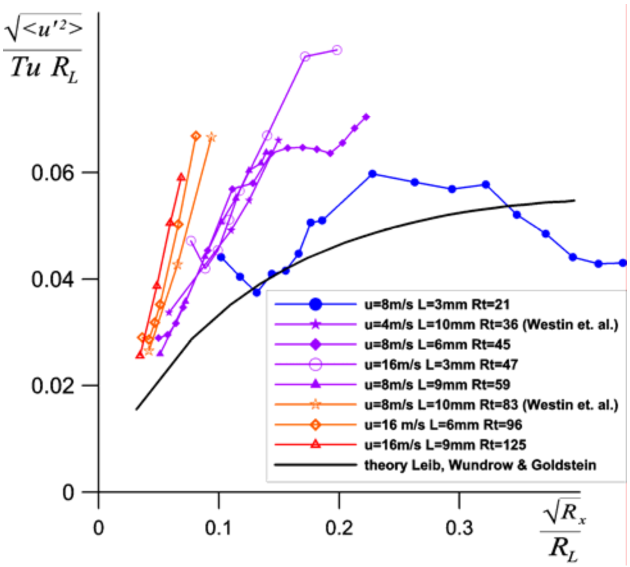

Fig. 3. Pulsations in the boundary layer on the plate with sharp leading edge normalized in accordance with (1).

General results of present experiment are the influence of magnitude of pulsations in boundary layer on the flat plate from turbulence scale or R_t and enhanced receptivity of the boundary layer on the blunt-nosed plate to FST. These results are explained theoretically in sections 3 and 4.

3. Receptivity of flat-plate boundary layer to FST

Discrepancy between the predictions of linear flat-plate boundary layer receptivity theory and experiment illustrated in previous section may be caused by non-linearity. There are two types of non-linear effects in the FST-induced transition: non-linear evolution of vortical disturbances in outer flow and non-linear development of streaky structures in the boundary layer. Here we shall account the first type of non-linear effects and describe the linear development of disturbances in boundary layer initiated by non-linear turbulence in the outer flow. Let's consider the interaction of grid turbulence with the boundary layer at infinitely thin plate located in the right part of *(x,y)* plane. The oncoming flow has mean velocity u_∞ which is directed along the x axis and r.m.s. pulsations $u' = Tu\,u_\infty$. We introduce non-dimensional variables using free-stream velocity and viscose length $l = \nu / u_\infty$ as scales. In these variables all coordinates are equal to the corresponding Reynolds numbers.

Vorticity field of FST will be presented as a superposition of periodic in space and time vortical modes. Two types of these modes: streamwise mode $\mathbf{\Omega}_{\|}$ with predominantly streamwise vorticity component and cross-flow mode $\mathbf{\Omega}_{\perp}$ with normal to flow direction vorticity will be considered.

$$\mathbf{\Omega}_{\|} = a(x)\left\{\mathbf{i}_0 - \frac{\alpha}{\beta}\mathbf{j}_0\right\}e^{i(\mathbf{k},\mathbf{r}-\tilde{\omega}t)}$$
$$\mathbf{\Omega}_{\perp} = a_{\perp}(x)\left\{-\frac{\gamma}{\beta}\mathbf{j}_0 + \mathbf{k}_0\right\}e^{i(\mathbf{k},\mathbf{r}-\tilde{\omega}t)} \qquad (2)$$

Here $\mathbf{i}_0, \mathbf{j}_0, \mathbf{k}_0$ are unit vectors along *x,y,z* axes, $\mathbf{k}$ is wavevector of vortical mode and α, β, γ - are streamwise spanwise and vertical wavenumbers, $\tilde{\omega}$ - is frequency . Streamwise and cross-flow modes correspond to modes « B » and « A » from [4]. Further it is assumed that spanwise and vertical periods of vortical modes are large, so cross-flow wavenumbers are small and will be considered as small parameters $\beta \sim \gamma << 1$. Low-frequency disturbances with $\alpha \sim \tilde{\omega} \sim \beta^2$ will be considered further because such perturbations exhibit maximal algebraic growth in the boundary layer [5, 6]. Because of flat-plate boundary layer is most receptive to streamwise vortisity, only streamwise modes will be considered further in this section.

In classical linear receptivity theory the interaction between vortical modes is neglected and they correspond to solutions of linearized Navier-Stokes equations. Amplitude of such modes decays exponentially and they are convected with free-stream velocity, so $\widetilde{\omega} = \alpha$. In real turbulence vortical disturbances decay more slowly and their phase speed deviates from the free-stream velocity. For this reason we shall consider vortical modes (2) with arbitrary dependence of amplitude from x and detuned frequency $\widetilde{\omega} = \alpha + \omega$. Such modes can not exist without the interaction with other part of spectrum of FST. The action of other disturbances to the mode will be replaced by the external force $\boldsymbol{F}$

$$\mathbf{F} = \left[\frac{da}{dx} + \left(\beta^2 + \gamma^2 - i\omega\right)a\right]\mathbf{v}_i \qquad (3)$$

which can be expressed in terms of velocity $\mathbf{v}_i$ induced by this mode of unit amplitude.

When the vortical mode interacts with flat plate without skin friction the perturbations of velocity can be found as a superposition of induced velocity in the free-stream and potential substituent found from the requirement that the vertical velocity should vanished at the plate. Because of potential substituent satisfies the linearized Navier-Stokes equations, the external force necessary for flow sustenance in the presence of the plate remains the same as in the free stream. If we have the plate with the boundary layer, the expression for external force (3) should be modified to account the displacement action of boundary layer. This can be made by substitution of stream function of basic flow in the boundary layer ψ for vertical co-ordinate z and some modification of the expression for induced flow velocity. Finally, the force in the presence of boundary layer is expressed by (3) with the following induced flow velocity

$$\mathbf{v}_i = \left[\gamma U_0 \mathbf{j}_0 + \beta \mathbf{k}_0\right] \frac{i}{\beta^2 + \gamma^2} e^{i(\alpha x + \beta y + \gamma\psi - (\alpha+\omega)t)} \qquad (4)$$

Here $U_0(x,z)$ is streamwise velocity in the boundary layer. External force given by (3), (4) induces cross flow with the same distribution of streamwise vorticity along the streamlines as in the free stream with vortical mode (2). However, it is valid if the flow is assumed to be strictly uniform in the streamwise direction and only perturbations in normal to flow direction plane are taken into account. To our point of view, such force is rather good model describing the action of other part of turbulence on the vortical mode interacting with boundary layer.

In fact, vortical mode produces both perturbations of cross-flow and streamwise components of velocity. These disturbances $\mathbf{v}(x,y,z,t)$ are governed by Navier-Stokes equations linearized around the basic flow in the boundary layer $\boldsymbol{V_b}$. Due to large streamwise period of perturbations the streamwise pressure gradient can be neglected and these equations take form

$$\frac{\partial \mathbf{v}}{\partial t} + (\mathbf{V}_b, \nabla)\mathbf{v} + (\mathbf{v}, \nabla)\mathbf{V}_b = \nabla_\perp p + \Delta_\perp \mathbf{v} + \mathbf{F} \qquad (5)$$
$$(\nabla, \mathbf{v}) = 0$$

Here p is perturbation of pressure, $\boldsymbol{F}$ – external force given by (3), (4), $\nabla_\perp, \Delta_\perp$ are gradient and Laplace operators in the cross-flow plane. The same equations without force were used for analysis of algebraically growing perturbations in [5, 6] and in linear receptivity theory [3]. This set of equations is of parabolic type, so initial conditions for $x=0$ and boundary conditions at the plate and in the outer flow are necessary. No-slip conditions are set at the plate, initial and outer flow conditions correspond to cross-flow velocity induced by vortical mode (4). For further consideration it is convenient to present the solution of (5) in the following functional form

$$\mathbf{v} = a(0)\left[\frac{1}{\beta^2} U \mathbf{i}_0 + \frac{1}{\beta} V \mathbf{j_0} + \frac{1}{\beta} W \mathbf{k}_0\right] e^{i(\beta y - (\overline{\alpha} + \overline{\omega})T)}$$
$$\{U,V,W\} = \{U,V,W\}(X, \eta, \overline{\alpha}, \overline{\omega}, \Gamma) \qquad (6)$$
$$X = \beta^2 X; \quad \eta = z/\sqrt{X}; \quad T = \beta^2 t$$
$$\overline{\alpha} = \alpha/\beta^2; \quad \overline{\omega} = \omega/\beta^2; \quad \Gamma = \gamma/\beta$$

where normalized velocity components U,V,W, coordinates X,η, wavenumber $\overline{\alpha}$ and frequency $\overline{\omega}$ are values of order of unity.

Based on solution for single vortical mode, boundary layer velocity pulsations from oncoming turbulence with spectral density of streamwise vorticity $<\omega_x^{\ 2}>(\mathbf{k})$ can be expressed as an integral

$$<u'^2>=$$
$$\int\int\int_{-\infty}^{+\infty}\frac{<\omega_z^{\ 2}>(\mathbf{k})}{\beta^4}\left\{\int_{-\infty}^{+\infty}S(\mathbf{k},\omega)\left|U_{\perp}\left(\beta^2 x,\eta,\frac{\alpha}{\beta^2},\frac{\gamma}{\beta}\right)\right|^2 d\omega\right\}\mathbf{dk} \qquad (7)$$

Here $S(\mathbf{k},\omega)$ is the density of frequency-spectrum of each harmonics of **k-** spectrum of streamwise vorticity in the frame of reference moving with free-stream velocity.

For isotropic turbulence and small α spectral density of streamwise vorticity is related to 3d energy spectrum *E(k)* as

$$<\omega_x^{\ 2}>(\alpha,\beta,\gamma)\cong<\omega_x^{\ 2}>(0,\beta,\gamma)=\frac{1}{4\pi}E(\sqrt{\beta^2+\gamma^2})$$
$$E(k)=Tu^2LF(k_1);\quad k_1=kL \qquad (8)$$

where $F(k_1)$ is normalized 3d energy spectrum which is approximated by Karman's spectrum

$$F(k_1)=\frac{15}{12\pi}\frac{k_1^{\ 4}}{(1+k_1^{\ 2})^{17/6}}$$

Frequency spectrum $S(\mathbf{k},\omega)$ was not ever measured directly or find from DNS of freely decaying turbulence. However, it can be normalized by characteristic correlation time of velocity pulsations in the frame of reference moving with flow velocity τ

$$S(\mathbf{k},\omega)=\tau\overline{S}(\omega\tau) \qquad (9)$$
$$\overline{S}(\omega\tau)=\frac{1}{\sqrt{\pi}}e^{-\frac{1}{2}(\omega\tau)^2}$$

Normalized spectral function $\overline{S}$ responsible for the shape of the time-spectrum is unknown and Gaussian distribution was chosen for its approximation. The correlation time τ was estimated in [7] and following analytical expression related this time with 3d energy spectrum was proposed here

$$\tau=\lambda\frac{L}{Tu}G(k_1)$$

$$G(k_1)=\left[\sqrt{I_c}+2\sqrt{I_R}+\sqrt{I_D}\right]^{-1}$$
$$I_c=k_1^{\ 2}\int_0^{k_1}F(k)dk;\quad I_R=\int_0^{k_1}k^2F(k)dk \qquad (10)$$
$$I_D=\int_{k_1}^{\infty}\frac{1}{k^2}F(k)dk$$

Coefficient λ in this expression is not determined and will be treated as an empirical constant. From (9), (10) the following expression for frequency spectrum was obtained

$$S(\mathbf{k},\omega)=\frac{\lambda L}{TuG(k_1)}\overline{S}\left(\frac{\lambda}{Tu}G(k_1)\omega_1\right);\quad \omega_1=\omega L$$

Amplitude of vortical mode which is used for computation of function *U*, describing disturbances produced by it in the boundary layer, was found from spectral density of streamwise vorticity and time-spectrum as

$$a(\mathbf{k},\omega,x)=\left(<\omega_x^{\ 2}>(\mathbf{k},x)S(\mathbf{k},\omega,x)\right)^{1/2} \qquad (11)$$

It depends from x indirectly through the dependence from x of turbulence intensity and scale. In subsequent computations the experimental data for *Tu(x)* was used and dependence of integral scale from x was found from well-known law $Tu^2L^3=const$.

Substitution of non-dimensional variables (6) for $\alpha,\beta,\gamma,\omega$ in integral (7) gives the following expression for r.m.s. velocity pulsations in boundary layer

$$\frac{\sqrt{<u'^2>}}{Tu_0\sqrt{L_0}}=\Phi(\overline{x},R_t);\quad \overline{x}=\frac{x}{L_0^{\ 2}};\quad R_t=Tu_0L_0 \qquad (12)$$

where Tu_0, L_0 are turbulence intensity and scale at the leading edge and R_t is turbulent Reynolds number. Normalized amplitude of pulsations

(12) appears in form of convolution of 3d energy spectrum and kernel function $R(X,k_1)$.

$$\Phi(\bar{x},R_t)=\left[\int_0^\infty \frac{F(k_1)}{k_1}R(k_1{}^2\bar{x},k_1)dk_1\right]^{1/2}$$

$$R(X,k_1)=\frac{\lambda k_1{}^2 G(k_1)}{\pi R_t}\int_0^\infty d\bar{\alpha}\int_{-\infty}^{+\infty} I(X,k_1,\bar{\alpha},\bar{\varpi})d\bar{\varpi} \quad (13)$$

$$I=\int_{-\infty}^{+\infty}\frac{1}{1+\Gamma^2}\left|U\left(\frac{X}{1+\Gamma^2},\bar{\alpha},\bar{\varpi},\Gamma\right)\right|^2 \bar{S}\left(\frac{\lambda k_1{}^2 G(k_1)}{R_t\left(1+\Gamma^2\right)}\bar{\varpi}\right)d\Gamma$$

Empirical constant λ was determined from experimental data by the following procedure. At first, amplitude of pulsations in boundary layer for $a(x)=const$ and $\lambda=1$ was computed. In the case of constant amplitude of vortical mode normalised velocity perturbations in boundary layer U are independent from the turbulent Reynolds number, and r.m.s pulsations for each R_t can be find without additional computations. In fact normalized pulsations amplitude in this case is function of $\bar{x}$ and the ratio R_t/λ. Constant $\lambda=0.2$ was found from the best fit of these solutions with experimental data for relatively small distance from leading edge where turbulence intensity and length scale are almost constant.

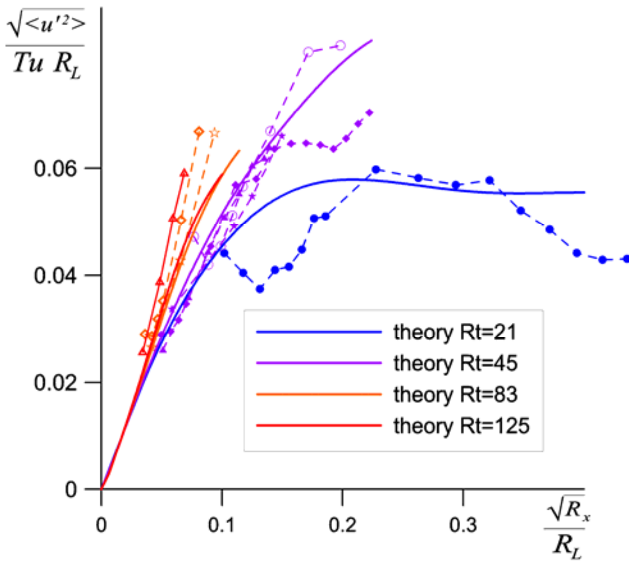

Fig. 4. Pulsations in the boundary layer on the plate with sharp leading edge normalized in accordance with (1). Experimental data denoted by symbols similar to fig. 3. Thick solid lines – results of non-linear receptivity theory.

Amplification curves of pulsations in the boundary layer for decaying turbulence (*a(x)* found from (11)) were computed for the most representative experimental cases in each color group: grid #1, u_∞=8m/s, R_t=21; grid #2, u_∞=8m/s, R_t=45; data of Westin et. al for u_∞=8m/s R_t=83 and grid #3, u_∞=16m/s, R_t=125. These curves together with experimental results are shown in Fig. 4. Coincidence of developed non-linear receptivity theory with experiment is rather good in comparison with linear receptivity theory by Leib, Wundrow & Goldstein [3]. Main advantage of present theory is qualitative description of the enhancement of amplification coefficient with the growth of turbulent Reynolds number. However, theory underestimates this trend.

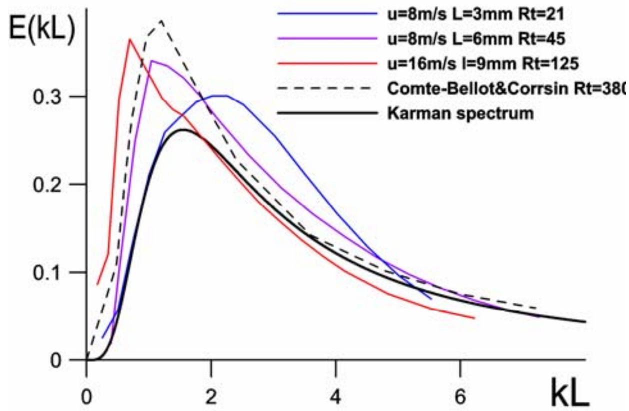

Fig. 5. Comparison of experimental 3d energy spectra and Karman spectrum.

Possible reason of inconsistence of theory with experimental data is incorrect model of 3d energy spectrum. Unfortunately, there are no reliable data concerning this spectrum for grid turbulence and its dependence from turbulent Reynolds number. Small number of these data is caused by the difficulty of finding of 3d-spectrum from measured 1d energy spectrum E_1. In accordance with relation between these spectra

$$E(k)=k^3\left(\frac{d}{dk}\left(\frac{1}{k}\frac{dE_1}{dk}\right)\right)$$

not perfect experimental spectrum should be differentiated two times. Available data concerning 3d-spectrum of turbulence are presented in Fig. 5. All measured 3d spectra deviate widely from the Karman spectrum used in the present theory. The trend of shift of maximum of the spectrum to smaller k_1 with R_t is seen from the spectra measured in present work, however spectrum found in [7] for R_t =380 do not reinforce this trend. The only definite conclusion follows from these data is that the 3d spectrum of grid turbulence is not universal when it is scaled by the integral scale. Additional information about this spectrum is necessary for verification of present receptivity theory.

4 Linear receptivity of boundary layer at blunt-nose plate to FST

Consider the velocity perturbations produced by free-stream turbulence in a boundary layer at the flat plate with blunt leading edge. Here linear model of FST will be used and attention will be paid on the vorticity field deformation by the flow around the leading edge. Goldstein [2] showed that interaction of vertical vorticity with blunt edge results to production of strong streamwise vortices above the boundary layer. For this reason the blunt-nosed plate boundary layer should be most receptive to cross-flow vortical mode $\mathbf{\Omega}_\perp$ and action of streamwise modes on it can be neglected. For this reason we shall consider here oncoming disturbances as a linear combination of cross-flow modes. Tese modes are considered as solutions of linearized Navier-Stokes equations without any external forces. It means that the frequency of the mode is equal to streamwise wavenumber and its amplitude decays exponentially as $\exp(-(\beta^2+\gamma^2))$.

The length of the plate is chosen such that the boundary layer thickness is comparable with period of mode but it is small with respect to nose radius. Matched asymptotic expansions method is applied to the problem under consideration and flow is divided into two regions shown in Fig. 6.

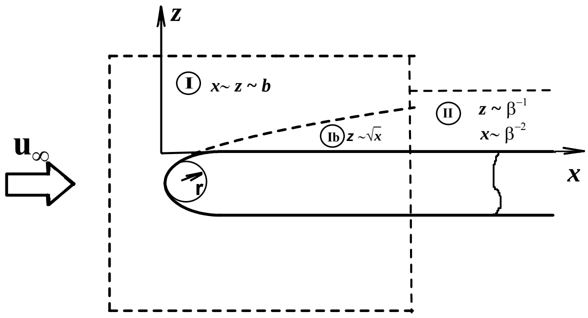

Fig. 6. Flow regions used for finding the disturbances in the boundary layer on the blunt-nose plate excited by cross-flow vortical mode.

In the vicinity of the leading edge where $x \ll \beta^{-2}$ (region I) the flow is inviscid outside a boundary layer of thickness $z \sim \sqrt{x}$ which is denoted as subregion I b. In this region vorticity field deformation takes place. Rapid distortion theory is used for finding of solution here. Interaction of cross-flow vortical mode with blunt leading edge leads to origination of infinite perturbations of spanwise velocity on the wall which behave as

$$w \to \frac{r}{2} a_\perp \ln(i\gamma - \beta z); \quad x >> r, \quad z \to 0$$

Logarithmical singularity at the wall is removed by viscosity in the boundary layer and it is not significant for subsequent consideration. However, spanwise velocity above the boundary layer is grater than oncomint perturbations of streamwise velocity by factor $\beta r >> 1$. It is cased by effect of amplification of disturbances by means of vortical tubes “wrapping”on the leading edge and vortex lines stretching highlighted in [2]. Further downstream in viscose region II perturbations of spanwise velocity are transformed into pulsations of streamwise velocity by lift-up effect.

Further analysis reveals that solution for streamwise velocity perturbations excited by cross-flow vortical mode in viscose region II takes the following functional form

$$u_\perp = a_\perp \frac{r}{2\beta} U_\perp\left(\beta^2 x, \eta, \frac{\alpha}{\beta^2}, \frac{\gamma}{\beta}\right); \quad \eta = \frac{z}{\sqrt{x}} \quad (14)$$

Normalized amplitude of velocity perturbations $U_\perp$ is a universal function of its four arguments. It was found by means of numerical solution of linearized Navier-Stokes equations with omitted longitudinal pressure gradient term (5) and ***F***=0. Normalized disturbances are maximal for $\alpha=\gamma=0$ and decrease with growth of spanwise wavenumber (frequency) and γ. For fixed α and γ this function grow as $U_\perp \sim \beta^2 x$ for small $\beta^2 x$, reaches maximum for $\beta^2 x \sim 1$, and decays for large $\beta^2 x$.

Based on solution for single vortical mode, boundary layer velocity pulsations from oncomong turbulence with spectral density of vertical vorticity $<\omega_z^{\ 2}>(\mathbf{k})$ can be expressed as an integral

$$<u'^2>= \frac{r}{2}\int\int\limits_{-\infty}^{+\infty}\int \frac{<\omega_z^{\ 2}>(\mathbf{k})}{\beta^2} U_\perp^{\ 2}\left(\beta^2 x, \eta, \frac{\alpha}{\beta^2}, \frac{\gamma}{\beta}\right)\mathbf{dk} \quad (15)$$

Spectral density of vertical vorticity component can be related to the 3d energy spectrum *E(k)*

$$<\omega_z^{\ 2}>=\frac{Tu^2}{4\pi}\frac{\beta^4}{\left(\beta^2+\gamma^2\right)^2}E(k)$$

Sabstitution of this into (15) gives the following expression for r.m.s. pulsations in the boundary layer on the plate with blunt leading edge

$$u' = \frac{Tu\, r}{\sqrt{L}}\Phi_\perp\left(\frac{x}{\sqrt{L}}, \eta\right)$$
$$\Phi_\perp = \left[\int\limits_0^\infty k_1 E(k_1) H_\perp\left(k_1^{\ 2}\bar{x}, \eta\right) dk_1\right]^{1/2} \quad (16)$$

It appears in form of convolution of energy spectrum of FST and kernel function $H_\perp$ defined as

$$H_\perp(X,\eta)= \frac{1}{2\pi}\int\limits_0^\infty\left[\int\limits_{-\infty}^{+\infty}\frac{1}{1+\Gamma^2}U_\perp^{\ 2}\left(\frac{X}{1+\Gamma^2}, \eta, \Gamma, \Omega\right)d\Gamma\right]d\Omega$$

Universal function $\Phi_\perp$ describing amplification of velocity pulsations in the boundary layer on the infinitely thin and blunt-nose plates are plotted in Fig. 7. It shows principal difference between pulsations behavior on thin and thick plates. Pulsations on the thin plate for Karman spectrum of turbulence (shown by thick solid line in Fig. 7) grow relatively slow and reach maximum $\sim 0.06\sqrt{L}$ far from leading edge where boundary layer thickness $\delta \sim \sqrt{x}$ becomes comparable with turbulence scale. Special analysis reveals that near the leading edge $u' \sim Tu\, L^{-1/3} x^{5/12}$ for $x << L^2$. This result slightly deviates from well-known growth proportional to $\sqrt{x}$.

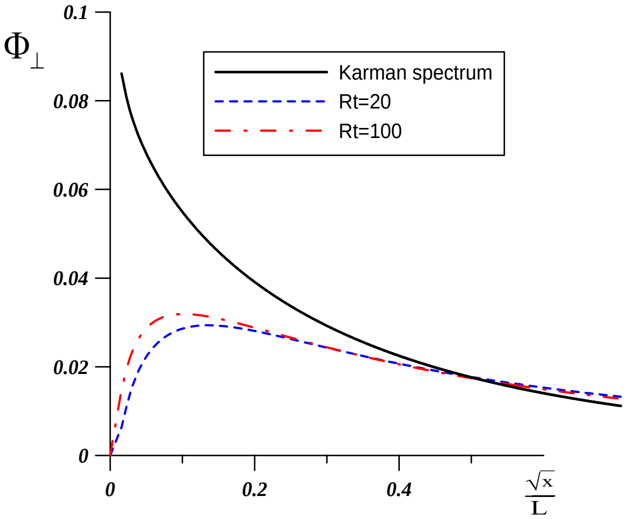

Fig.7. Universal functions describing growth of pulsations induced by FST in the boundary layer on the plate with blunt leading edge.

For the same Karman spectrum of FST, maximal amplification of pulsations at the blunt-nose plate takes place near the leading edge. Asymptotic analysis shows that $H_\perp \sim \sqrt{X}$ for small X and pulsations near the leading edge behave as $u' \sim Tu\, r\, L^{-1/3} x^{-1/12}$ for $x << L^2$. Singularity on the leading edge can be removed if more complicated model of energy spectrum including the exponential decay in the viscose range is used instead of Karman spectrum

$$E(k_1) = k_1^3 \frac{d}{dk_1}\left(\frac{1}{k_1}\frac{dF}{dk_1}\right); \; F(k_1) = \frac{1}{\pi}\frac{e^{-ak_1}}{1+bk_1^{5/3}}; \quad (17)$$
$$a = 5.6R_t^{3/4}; \quad b = \frac{1.35}{1+35R_t^{-3/4}}$$

Universal amplification functions $\Phi_\perp$ computed with this energy spectrum for $R_t = 20$ and 100 are also plotted for in fig. 7. They nearly coincide and have maxima in the vicinity of the leading edge. Maximal amplification of pulsations on the blunt-nose plate is scaled as $\sim 0.03r/\sqrt{L}$ and is reached at $x \sim 0.01L^2$. Large difference between the results found with Karman spectrum and real spectrum (17) is explained by dominant contribution of small-scale perturbations into total r.m.s. pulsations near the blunt leading edge.

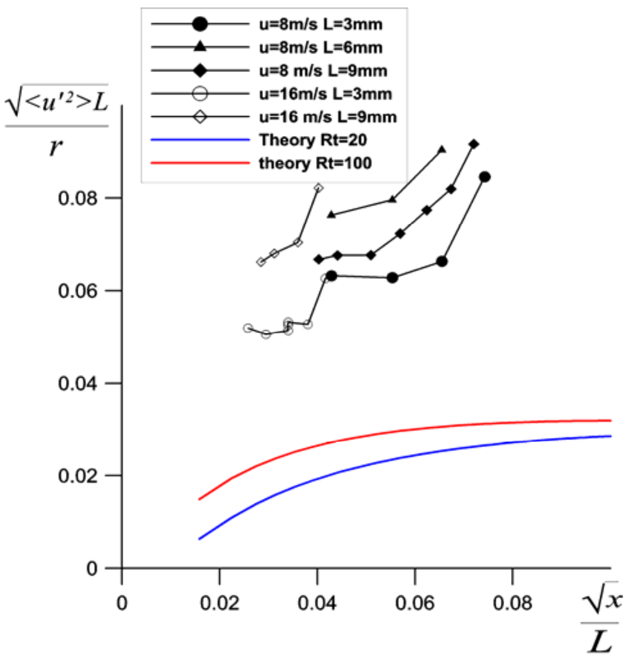

Fig.8. Comparison of normalized disturbances on the blunt-nose plate with theory

Fig. 8 compares theory developed here with experimental data obtained with blunt-nosed plate which are described in section 2. Only initial part of amplification curves which is near to constant and first few points in the region of non-linear growth are shown in this figure. Fig. 8 shows that beginnings of amplification curves of pulsations scaled with accordance with (16) lie near to each other. However they diverge when non-linear growth of pulsations starts. Similarly to the case of flat plate, linear receptivity theory underestimates magnitude of velocity pulsations in boundary layer by factor of 2-3. This theory can be improved if the non-linearity of FST would be taken into account in manner described in the previous section. Development of such non-linear receptivity theory for blunt-nosed plate is in progress now.

In flight conditions and in the experiments performed in industrial wind-tunnels the turbulence scale is large with respect to boundary layer thickness. Asymptotic behavior of disturbances for $x << L^2$ found for real energy spectrum is required for correct theoretical description of transition in these conditions. Such analysis shows that in the boundary layer on the thin plate disturbances near the leading edge take form

$$u' \approx Tu\sqrt{I_1}\sqrt{\frac{x}{L}}; \qquad I_1 = \int_0^\infty k_1 F(k_1)dk_1$$

The integral here can be estimated as $I_1 \sim R_t^{1/4}$ (see [8]) and following final expression for disturbances may be obtained

$$u' \sim A\,Tu\sqrt{\frac{x}{L}}R_t^{1/8}$$

Here A is an universal constant. Similar asymptotic analysis for the blunt-nose plate gives

$$u' \approx \frac{Tu\,r}{L}x^{1/4}\sqrt{I_2}; \qquad I_2 = \int_0^\infty k_1^2 F(k_1)dk_1$$

Integral $I_2 \sim R_t$ and asymptotic behavior of pulsations near the blunt leading edge takes form

$$u' \sim B\frac{Tu\,r}{L}R_t\,x^{1/4}$$

with another universal constant B. The ratio of amplitude of disturbances on the blunt-nose plate to the same value for thin plate is proportional to

$$u'_{blunt} / u'_{thin} \sim \frac{r}{\sqrt{L}} R_t^{7/8} x^{-1/4}$$

Estimates shows that for typical flight conditions ($u'_\infty \approx 200 m/s$, $r' = 2cm$, $L = 10m$, $u' = 1m/s$, $x=1m$) pulsations on the blunt-nose plate exceeds this for the thin plate by factor 10^4. Similar estimate for experiment in transonic wind-tunnel ($u'_\infty \approx 200 m/s$, $r' = 0.2cm$, $L = 0.2m$, $u' = 1m/s$, $x = 0.1m$) gives $u'_{blunt} / u'_{thin} \sim 20$. These examples demonstrate the importance of effect of leading edge on laminar-turbulent transition excited by FST.

Acknowledgments

The work was made with financial support of RFBR (grant #10-08-01271-a)

References

[1] Westin K.J.A., Boiko A.V., Klingmann B.G., Kozlov V.V., Alfredsson P.H. Experiments in a boundary layer subjected to free-stream turbulence. Pt. I: Boundary layer structure and receptivity. *J. Fluid Mech*. Vol. 281, pp 193-218, 1994.
[2] Goldstein M.E., Leib S.J., Cowley S.J. Distortion of a flat-plate boundary layer by free-stream vorticity normal to the plate *J. Fluid Mech*. Vol. 237, pp 231-260, 1992.
[3] Leib S.J., Wundrow D.W., Goldstein M.E. Effect of free-stream turbulence and other vortical disturbances on laminar boundary layer, *J. Fluid Mech* Vol 380, pp 169-203, 1999.
[4] Bertolotti F.P. Response of the Blasius boundary layer to free-stream vorticity, *Phys. Fluids* Vol 9, pp 2286-2293, 1997
[5] Andersson P., Berggren M., Henningson D.S. Optimal disturbances and bypass transition in boundary layers. *Phys. Fluids*. Vol 11, pp 134-142, 1999
[6] Luchini P. Reynolds-number-independent instability of the boundary layer over a flat surface: optimal perturbations, *J. Fluid Mech*. Vol 404, pp 289-302, 2000
[7] Comte-Bellot G., Corrsin S. Simple Eulerian time correlation of full- and narrow-band velocity signals in grid-generated "isotropic" turbulence *J. Fluid Mech*. Vol 48, pp 273-337, 1971
[8] Gyiliaev A.N., Kozlov V.E., Kuznetsov V.R. Penetration of three-dimensional low-frequency outer-flow velocity pulsations into flat-plate boundary layer. in: *Trudi TsIAM*, No 1287, pp 197-236, 1991 (in Russian)

Copyright Statement

The authors confirm that they, and/or their company or organization, hold copyright on all of the original material included in this paper. The authors also confirm that they have obtained permission, from the copyright holder of any third party material included in this paper, to publish it as part of their paper. The authors confirm that they give permission, or have obtained permission from the copyright holder of this paper, for the publication and distribution of this paper as part of the ICAS2012 proceedings or as individual off-prints from the proceedings.